Desalination and Water Treatment
www.deswater.com

doi:10.5004/dwt.2017.20896

82 (2017) 271–281
July

Phosphate removal from aqueous solutions using magnetic multi-walled carbon nanotube; optimization by response surface methodology

Vahid Alimohammadi[a], Mehdi Sedighi[b,*], Ehsan Jabbari[a], Mahmoud Nasrollahzadeh[c,d]

[a]*Department of Civil Engineering, University of Qom,Ghadir Boulevard, Postal Code 3716146611, Qom, Iran, email: alimohamadi.vahid@yahoo.com (V. Alimohammadi), e.jabbari@qom.ac.ir (E. Jabbari)*
[b]*Department of Chemical Engineering, University of Qom, Ghadir Boulevard, Postal Code 3716146611, Qom, Iran, Tel. +98 2532103520, email: sedighi@qom.ac.ir (M. Sedighi)*
[c]*Department of Chemistry, Faculty of Science, University of Qom, Ghadir Boulevard, Postal Code 3716146611, Qom, Iran, email: mahmoudnasr81@gmail.com (M. Naasrollahzadeh)*
[d]*Center of Environmental Researches, University of Qom, Ghadir Boulevard, Postal Code 3716146611, Qom, Iran*

Received 8 October 2016; Accepted 10 May 2017

ABSTRACT

This work presents the application of magnetic multi-walled carbon nanotubes (MMWCNTs) for the removal of phosphate from aqueous solutions. Prepared nanoparticles were characterized by TEM, FTIR, VSM, and XRD measurements. The prepared magnetic adsorbent can be well dispersed in the aqueous solutions and quickly separated from the medium after loading on the adsorbent by a magnet. The application of response surface methodology (RSM) was investigated for optimizing the removal of phosphate from aqueous solutions using MMWCNTs. The effects of D/C (adsorbent dosage per initial concentration of pollutant ((mg) $_{adsorbent}$/(mg/l) $_{initial}$) and initial pH on phosphate removal (%) evaluated by RSM. Using RSM methodology, a quadratic polynomial equation was used for the removal of phosphate by multiple regression analysis. The optimum removal of phosphate was 97.35% at pH = 4 and D/C = 2.50. The experimental data were analyzed by the Langmuir and Freundlich adsorption models. The Maximum adsorption capacity for phosphate removal was obtained as 256 mg·g^{-1} from the Langmuir is other mmodel. The present work indicates the novel nature of the MMWCNT, which can remove the phosphates from the water.

Keywords: Phosphate removal; Multi-walled carbon nanotubes; Magnetic; RSM; Isotherm models

1. Introduction

As water is a vital resource, water pollution is a serious issue for human beings ecosystems [1,2]. For different applications, the water must be free of germs and chemicals and be clear. The main sources of water available to use are wells, lakes, rivers, and surface water. Industrials' wastewater and effluent from agriculture and animal husbandry activities contribute to the accumulation of contaminants in soil and water bodies [3]. Wastewater purification is important because of generating a great volume of urban and industrials that produce wastewaters in industrialized countries, and maybe released these wastewaters into environmental [4]. Among the different contaminants, nutrient pollution is one of the most widespread, costly and challenging environmental problems. Phosphorus (P) is a nutrient that is a common constituent of agricultural for fertilizer, manure, and organic wastes in sewage and industrial effluent. Total Phosphorus (TP) concentration in treating effluents from municipal and industrial sources is usually less than 2.0 mg·L^{-1}, but it is often responsible for eutrophication leading to short- and long-term environmental and aesthetic problems in lakes, coastal areas, and other confined water bodies [5]. Phosphorus is a key nutrient that stimulates the growth of algae and other photosynthetic microorganisms such as toxic cyanobacteria [6].

The removal of phosphate from wastewaters and municipal pollutants is necessary to meet the tough stan-

*Corresponding author.

dards of WHO [7]. Various technologies, including filtration, biological, chemical and physical treatment have been investigated for the removal of phosphate from wastewaters [8]. Phosphor removed from spiked municipal wastewater using either electrochemical coagulation or chemical coagulation as tertiary treatment. The researchers indicated that at least, 97% of total phosphorus in the range of 5–50 mg/l was removed from municipal wastewater. The optimal conditions as energy consumption, electrode consumption, metallic sludge disposal, the amount of MMCNT, initial concentration, and initial pH should be considered for P_{tot} removal [3,9]. The adsorption method could be a promising and a novel technology for the removal of pollutants such as phosphate in wastewater compared to other technologies, because this method can be produced quality water after wastewater treatment [10]. Hydrated ferric oxide (HFO) and hydrated zirconium oxide (HZRO) were able to reduce phosphate in a real wastewater [11]. Zhou et al. [12] investigated the removal of phosphate by HFO nanoparticles coated activated carbon fiber. The adsorption of phosphorus by hydrated ferric oxide (HFO) nanoparticles coated activated carbon fiber (ACF) prepared by Sol–Gel procedure. The results indicated that the (ACF-HFO) NPs had a high performance for the adsorption of phosphorus from wastewaters. Total phosphorus (TP) adsorption capacities improved according to increases in loess dosage, initial concentration, agitation rate and temperature [13]. However, TP removal efficiencies decreased when pH is high and loess particle becomes large. The results obtained from this work shown that loess is an applicable adsorbent for the removal of TP of the municipal wastewater. Generally, P removal increased with the adsorbent dose rate. Column flow-through tests using a secondary effluent confirmed the results carried out from the batch experiment. The adsorption rates of dissolved phosphate (DP) and (TP) by a peat column from the secondary effluent were good. These results suggested that based on large surface area and high amorphous Fe and Al contents, peat possessed great potential for its use as substrate bed material for the adsorption of phosphorus from secondary wastewaters [3]. Phosphorus removal from wastewater by adsorption method could be more suitable than precipitation in the removal of phosphorus. As shown, the column experiments, about 65% of phosphorus can be retained through adsorption by goethite coated silica sand [14].

Among various adsorbents, multi-walled carbon nanotubes (MWCNTs)which is one of the types of carbon nanotubes [15] have attracted more attention to their unique structure, excellent mechanical, and thermal properties. Carbon nanotubes have attracted researchers' interest as a new type of powerful solid-phase extraction adsorbent because of their relatively large specific area [16]. Magnetic carbon nanotubes (CNTs) are usually prepared using the chemical deposition of Fe_3O_4 [17]. Furthermore, magnetic nanoparticles have been recognized as an effective adsorbent with the small diffusion resistance [10]. Magnetic MWCNTs could be used for the removal of pollutants from wastewater and after adsorption, can be separated from the solution by a simple magnetic process [16]. Adsorption is proven to be an economical and effective method for the removal of several contaminates from wastewater [18–22]. Response surface methodology design is a mathematical technique that could be useful to analyze various parameters as pH, initial concentration, and dosage adsorbent to achieve maximum removal [23]. Several studies investigated the removal of pollutants from wastewater using MMWCNTs, but there is not still many reports about the removal of phosphate from wastewater by magnetic MWCNTs. In this paper, the authors reported a facile method to prepare MWCNTs/Fe_3O_4 NPs composite nanotubes. It was to synthesize nearly monodispersed Fe_3O_4 NPs on the surface of MWNTs by an in situ method which a fine morphology was obtained. A simple and efficient method was introduced to remove the phosphates by MMWCNTs from wastewater. In addition, MWCNT/Fe_3O_4 NPs from wastewater have carried out the systematic study for the removal of phosphates.

2. Materials and method

The MWCNTs (the length of 5–15 μm and the average outer diameter was between 10–30 nm) were used in our experiment. MWCNT were purchased from Nano port Co. Ltd. (Shenzhen, China). Other reagents were of analytical grade and used without further purification including $FeCl_3{\cdot}6H_2O$, $FeCl_2{\cdot}4H_2O$, and $NH_3{\cdot}H_2O$. All glassware were soaked in dilute nitric acid for 24 h and finally washed for three times with DDW prior to use. The neodymium-iron- boron block magnet use in generating the magnetic field for sulfate water separation was used. (Maximum field strength: 13.2 KG). Ferric chloride hexahydrate ($FeCl_3{\cdot}6H_2O$, analytically pure), ferrous chloride ($FeCl_2$, analytically pure), ammonia solution (28 wt. %) and KH_2PO_4 were all bought from Merck. The Design Expert 7.5 software was used for regression and graphical analyses of the experimental data.

2.1. Synthesis of MWCNT/Fe_3O_4 magnetic nanoparticle

The MWCNTs were dispersed in concentrated sulfuric acid and nitric acid media (a 4:1 volume ratio) to modify the MWCNTs surface by ultrasonication for 3 h. The oxidized MWCNTs were filtered with a PTFE (Polytetrafluorethylene) filter membrane (Alltech, 0.45 μm pore size) with the aid of vacuum pump then washed by DW (deionize water) until the filtrate is neutralized. MWCNTs were dried in the oven at 80°C for 6 h. 30 mg of functionalized MWCNTs were dissolved in 21 ml of distilled water by ultrasonic irradiation for 25 min. Then 23 mg of $FeCl_3{\cdot}6H_2O$ was added under stirring. After the mixture was stirred vigorously for 25 min under N_2 atmosphere, 35 mg of $FeCl_2{\cdot}4H_2O$ was added and keep stirring under N_2 atmosphere for 25 min. 8 ml of concentrated $NH_3{\cdot}H_2O$ diluted with 17 ml of distilled water was added to the mixture drop by drop. The addition of $NH_3{\cdot}H_2O$ aqueous solution was finished in 2 h and then the solution heated to 80°C and reacted for 8 h. The whole process must be under N_2 atmosphere. The reaction mixture was then centrifuged, washed with distilled water for several times and dried at 70°C for 12 h.

2.2. Preparation of solution

Phosphate stock solution containing 2000 mg KH_2PO_4/L was prepared by dissolving KH_2PO_4 salt (analytical reagent

grade) in distilled water. Phosphate working solutions in various initial concentrations were prepared by diluting the phosphate stock solution with 0.01 M KCl for adjusting the ionic strength. The pH value of the P working solution was adjusted with 1 M HCl and 1 M NaOH solutions before adsorption experiments.

2.3. Instrument

The model of pH-meter is Metrohm-713 for this study. The concentration of residual phosphate in the flask was measured calorimetrically using a spectrophotometer (UV-DR5000, Hach). The absorbance was read at 880 nm. The method is analogous to EPA 365.2 + 3, US Standard Methods 4500-P E and ISO 6878.

2.4. Adsorption study

The adsorption of phosphate on MMWCNT was investigated under batch conditions. For this study, 12 series of solutions each containing 50 mL aqueous solution sample, and the various range of concentrations from 40 to 166.67 mg/l of phosphate with 0.005 g of the nanocomposite was blended for 60 min in 100 mL bottles kept in a shaker rotating with at rpm of 100. The temperature was kept at 25°C in preliminary experiments. The ionic strength of solution was adjusted to 0.01 mol/L using KCl.

The percentage of phosphate removal was obtained using the following equation [24]:

$$R\% = \frac{(C_0 - C_t)}{C_0} \times 100 \quad (1)$$

where C_o and C_t are the initial and final concentrations in mg/ L. The experiments were performed at room temperature. The supernatant solutions were analyzed spectrophotometrically at 880 nm wavelength. The effect of pH on the removal of phosphate by MMWCNTs was investigated. The range of initial pH values considered from 4–10. Phosphate adsorption on MMWCNT was calculated from Langmuir and Freundlich Isotherms.

2.5. Characterization

Chemical structure of γ-Fe_3O_4 nanoparticle functionalized with MWCNT was determined by XRD. XRD traces were recorded from 2θ of 20–70° with a 0.02° step size. Powder X-ray diffraction (XRD) patterns were measured using a Rigaku D/max-cB automatic X-ray diffractometer with a Cu Ka radiation (k = 0.154056 nm). Transmission electron microscopy (TEM) experiments were performed on a Hitachi 8100 electron microscope (Tokyo, Japan) and a JEM-2000. EX electron microscope with an acceleration voltage of 200 kV. Fourier transform infrared (FTIR) spectra of KBr powder-pressed pellets were recorded on an Agilent Cary 600 series FTIR spectrometer. VSM was employed to determine the magnetic saturation value of MWCNT-γ-Fe_3O_4 magnetic nanoparticles at room temperature. The specific surface area and pore size of MWCNTs and MMWCNTs were determined by nitrogen adsorption/desorption porosimetry at (77.4 K) using a porosimeter (Bel Japan, Inc.).

3. Result and discussion

3.1. Characterization of MWCNTs/Fe_3O_4 nanocomposites

The structure of MMWCNTs, γ-Fe_3O_4 and MWCNTs were investigated by powder XRD measurements and the powder diffraction pattern of MWCNTs are displayed in Fig. 1a. It is obvious The diffraction peaks at 2θ = 25.55° and 44.49° are consistent with (002), (100) planes of the MWCNTs. The peaks of γ-Fe_3O_4 are shown in Fig. 1b. Fig. 1c represents the XRD pattern of MMWCNTs that contains all the carbon nanotube and iron oxide nanoparticles peaks. The crystalline diffraction peaks at 2θ = 29.74, 35.25, 43.09, 57.09 and 62.67 corresponded to the (220), (311), (400), (511) and (440) planes of the spinel phase of Fe_3O_4 (JCPDS No. 65-3107), respectively [25]. The XRD results confirm that MWCNTs/Fe_3O_4 nanocomposites were successfully synthesized by a facile hydrothermal method and the existence of MWCNT and Fe_3O_4 in the nanocomposite.

The TEM images of the MMWCNTs presented in Fig. 2. Most of the MWCNTs were loaded with iron oxide nanoparticles. Fig. 2a shows that no separated nanoparticles were found on the TEM carbon nanotubes nanoadsorbent, which suggests that the unattached nanoparticles have been completely removed from the product. The image of MMWCNTs nanocomposites (Fig. 2b) confirms the good fabrication for the MMWCNTs nanocomposites. Some nanoparticles assembled into nanotubes but still adhered stably on the tube surface. There is no detected bare surface area on the surface MWCNTs, showing the high efficiency of our synthesis method.

Surface functionalities of synthesized MMWCNTs were investigated by considering the spectroscopic results from FT-IR studies. Fig. 3a and b of MMWCNTs and MWCNTs were carried out for a better comprehension of the structure and composition of these materials. An absorption band revealing the vibrational properties of the Fe–O bond is observed around 568 cm^{-1}. This band is mainly assigned to the stretching vibrations of Fe–O–Fe. The broad absorption peaks between 3400–3500 cm^{-1} correspond to –OH group, showing the hydroxyl groups on the surface of the composites or it can be attributed to the adsorption of some atmospheric water during FTIR measurements. The C=C band of aromatic ring appeared at 1621 cm^{-1} of the functional groups on the surface of the MWCNTs. The peak at 2940 cm^{-1} corresponds to the C–H stretch vibration, originated from the surface of MWCNTs.

The magnetic properties of the synthesized MMWCNTs are shown in Fig. 4a.The sample exhibits no coercivity and remanence, and its saturation magnetization is about 29.5 emu/g at 30 kOe. As-prepared MWCNT-iron oxide composites can be easily dispersed in water and form a stable dispersion which due to magnetic properties, these MWNT-iron oxide composites could be quickly separated from their dispersion holding the sample close to a commercial magnet. Fig. 4b indicates that it can be manipulated by an external magnetic field. From the results it could be said that MWCNT/Fe_3O_4 can be easily and reliably targeted through the specific applications.

Specific Surface area (SSA) of the MMWCNTs was analyzed commonly by The Brunauer, Emmett, and Teller (BET) method. The SSA of the sample is measured by physical adsorption of a gas on the surface of the solid and by

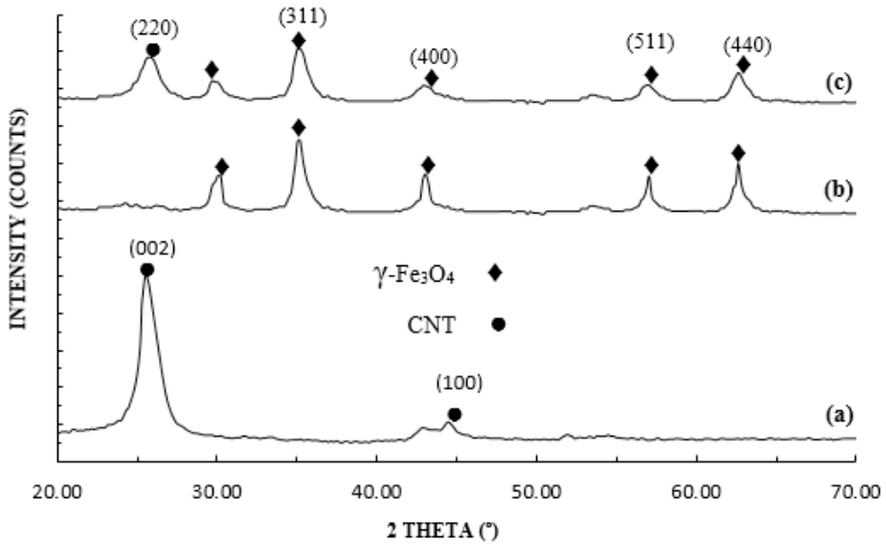

Fig. 1. Power XRD patterns of (a) MWCNTs, (b) γ-Fe_3O_4, (c) MMWCNTs.

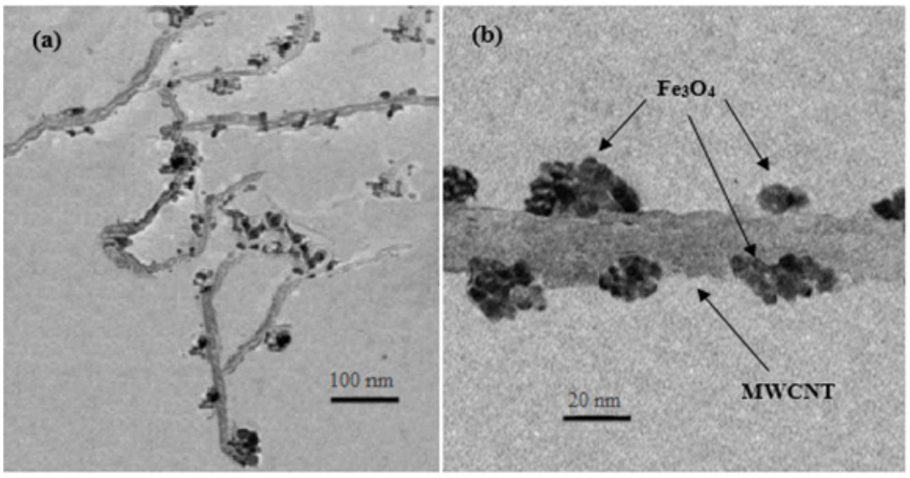

Fig. 2. Representative TEM image of MWCNT/Fe_3O_4nanocomposites (a, b).

measuring the amount of adsorbed gas corresponding to a monomolecular layer on the surface [10]. The BET measurements found that the SSA of MWCNTs and MWCNT/Fe_3O_4 were 127.91 m^2/g and 112.26 m^2/g, respectively. When the Fe_3O_4 particles are filled in the MWCNTs, the surface area of the MMWCNTs decreases slightly [16].

3.2. Experimental design

Response surface methodology (RSM) coupled central composite design (CCD) for two factors was considered for experimental design. We selected pH (X_1) and D/C (X_2) as control variables. D/C means the adsorbent dosage per initial concentration of pollutant ($(mg)_{adsorbent}/(mg/l)_{initial}$). The design consists of two-level full factorial design (2^2 = 4), four star points, and one center point. Furthermore, we carried out three reproduces at the central point to evaluate the pure error among each experiment. The order of experiments was randomized to lower the uncontrolled effect of factors. A second order equation was expanded to estimate the responses as a role of independent variables involving their quadratic interactions and squared terms. We coded the variables X_i as x_i according to Eq. (2):

$$x_i = \frac{X_i - X_0}{\Delta X_i} i = 1,\ 2,\ 3,\ \ldots,\ k \tag{2}$$

The basis of forming a second order equation in removal is given in Eq. (3):

$$Y = \beta_0 + \sum_{j=1}^{3} \beta_j X_j + \sum_{j=1}^{3} \beta_{jj} X_j^2 + \sum_{i<j} \beta_{ij} X_i X_j \tag{3}$$

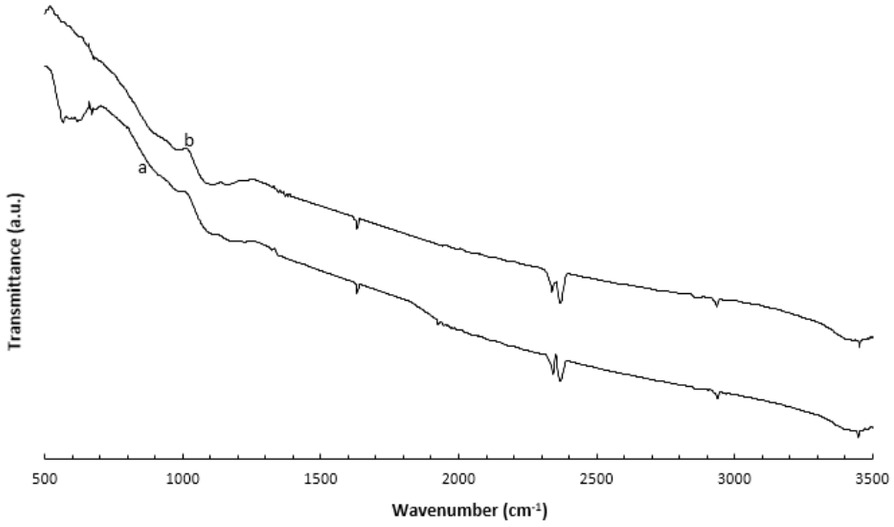

Fig. 3. The IR spectra of (a) MMWCNT, (b) MWCNT.

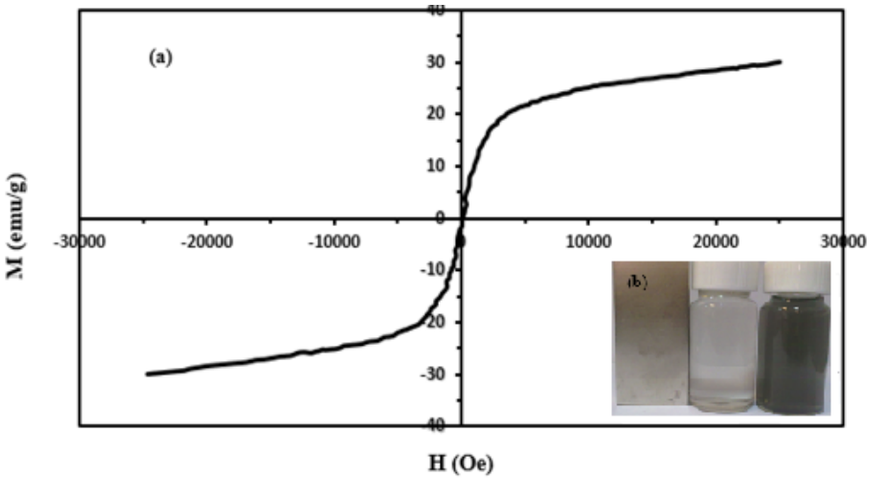

Fig. 4. (a) Magnetization curve at 25°C (300 K) of MWCNT-iron oxide composites. (b) Photograph of MWCNT-iron oxide composites dispersed in water (right) and their response to a magnet (left).

Multiple regression analysis techniques contained in the RSM were used to predict the coefficients of the models. The design factors and levels for both CCD studies are shown in Table 1; meanwhile, the design matrix with their corresponding results is listed in Table 2.

The resultant second-order models for the phosphate removal generated as shown in Eq. (4):

$$R_1 = +4.29301+3.52438\ X_1 + 12.14310\ X_2 - 6.05088\ X_1 X_2 + 0.03889 X_1^2 + 17.35734\ X_2^2 \quad (4)$$

The effects of the design parameters on phosphate removal can be determined by means of the ANOVA given in Table 3. The F value is a ratio of the mean square due to regression to the mean square due to error. P-values are associated with F values as they are useful to display whether F values are large enough to show the statistical significance. In the model, linear and quadratic parameters were significant with $P < 0.05$. The predicted R-Squared value is found 0.97 for equation. The value of R-squared is a measure of total variation of observed values about the mean explained by the fitted model. Therefore, R-squared shows very good fitting for experimental and estimated data.

The observed versus predicted values are illustrated in Fig. 5. It can be seen that most of the points of experimental values lie are close to the straight line as the predicted values.

3.3. Main factors effect

To observe all factors on one response plot, the perturbation plot can be used, which provides silhouette views of

the response surface (Fig. 6). For response surface designs, the perturbation plot shows how the response changes as each factor moves from the chosen reference point, with all other factors held constant at the reference value. In Fig. 6, reference points are set in the middle of the design space (the coded zero level of each factor). As shown, increasing pH results in reducing phosphate removal. Fig. 6 shows that increasing D/C results affect the increasing phosphate removal. The effect of pH and D/C on phosphate removal are completely different.

3.4. Contour plots

Authors analyzed the simultaneous effects of two independent variables, including pH and D/C on phosphate removal. Eq. (4) is used to construct the response surface and contour plots in which the second independent variable is in midpoint level. According to Fig. 7, increasing D/C and decreasing pH results in increasing phosphate removal. It approves that the pH and D/C are important parameters affecting the removal of phosphate. According to Fig. 8, the higher amount of pH and lower amounts of D/C lead to a more reduction of phosphate removal. Furthermore, an optimum point exists for pH and D/C. At pH = 10 and (D/C) = 0.6, the removal of phosphate reaches to a minimum value, and at pH = 4 and D/C 2.5 the removal of phosphate reaches the maximum value.

To validation the model optimization of phosphate removal, three more runs were performed and the final optimal points were compared with those from experimental data at same conditions. Table 4 shows the average relative error for phosphate yield is 2.75%.

Table 1
Coded levels and factors for CCD study

level	pH (X_1)	D/C (X_2)
−α	4.00	0.60
–1	4.88	0.88
0	7.00	1.55
+1	9.12	2.22
+α	10.00	2.50

Table 2
CCD experimental matrix data for removal study

Run	Factor		Final
	pH	D/C	Removal (%)
1	7.00	1.55	25.96
2	4.88	2.22	72.32
3	4.00	1.55	36.62
4	9.12	0.88	12.35
5	7.00	1.55	25.23
6	7.00	0.60	17.65
7	4.88	0.88	25.32
8	9.12	2.22	24.86
9	10.00	1.55	15.63
10	7.00	1.55	26.65
11	7.00	2.50	65.23
12	7.00	1.55	25.12

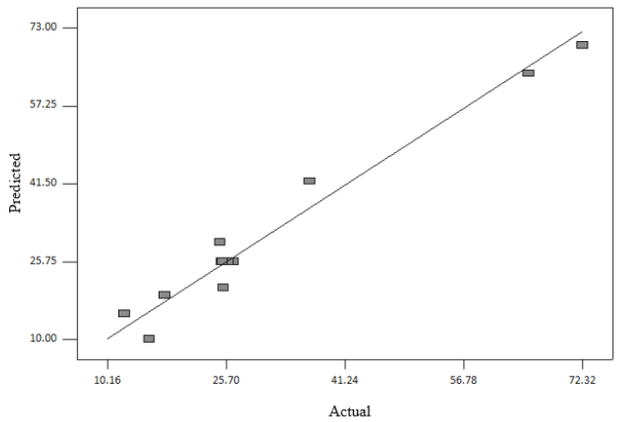

Fig. 5. Actual against predicted values for removal phosphate.

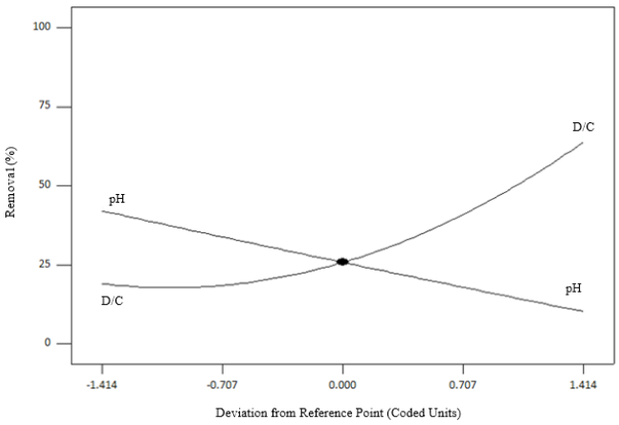

Fig. 6. Main effects of main parameters for the removal of phosphate.

Table 3
ANOVA for the removal of phosphate

Source	Sum of squares	Degree of freedom	Mean square	F_{Value}	P_{Value}	R^2
S.S. regression	3727.73	5	745.55	35.15	0.0002	0.97
S.S. error	127.26	6	21.21			
S.S. total	3854.99	11				

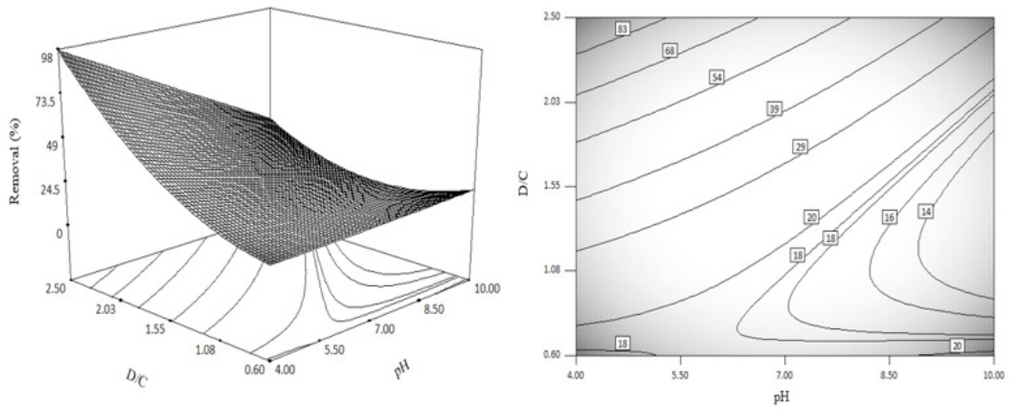

Fig. 7. 3D response surface plots and a counter graph of phosphate removal with varying pH and D/C.

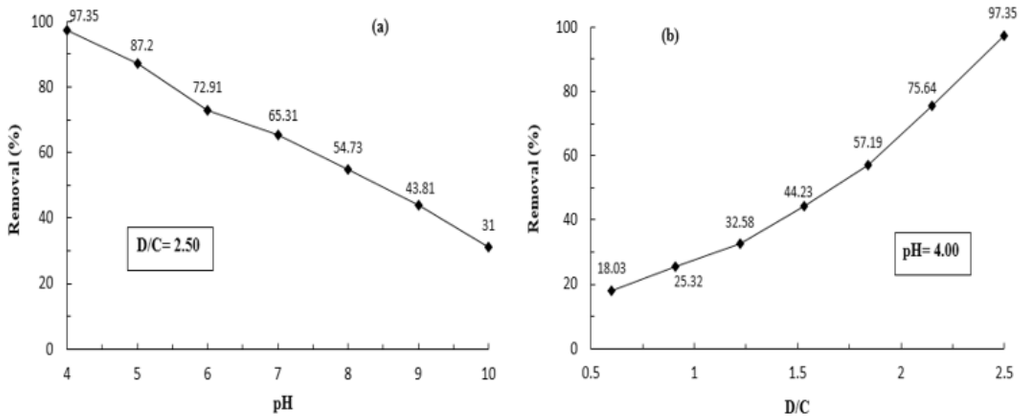

Fig.8. (a) Effect of pH, and (b) Effect of D/C on the phosphate removal.

Table 4
Result verification of the experiment and predicted values

Phosphate yield (wt %)				
Parameters		Y_{model}	$Y_{experiment}$	% Relative error
pH	D/C			
4.88	2.22	69.37	72.32	4.07
7.00	2.5	63.82	65.23	2.16
7.00	1.55	25.74	25.23	2.02
		%Average relative error		2.75

The pH of the solution is one of most controlling parameter during adsorption process [26], which affects the surface charge of the MMWCNTs. In order to establish the effect of pH, the equilibrium studies at various ranges of initial pH values were considered from 4–10. As shown in Fig. 8a, the pH of the solution has a high effect on the removal of phosphate. With an increment of pH from 4 to 10 at D/C 2.50, the removal (%) decreased from 97.35% to 31.00%. The maximum removal of phosphate by MMWCNT was obtained at pH 4.00 and D/C 2.50. Fig. 8b shows that with increasing of D/C, the removal of phosphate increased from 18.03% to 97.35%.Therefore, the pH and D/C values are important factors for phosphate removal.

3.5. Adsorption isotherms

The adsorption isotherms of phosphate by MWCNTs/Fe_3O_4 in aqueous solution can be analyzed using the Langmuir and the Freundlich adsorption models. In order to optimize the use of MMWCNTs adsorbents, it is important to establish the most suitable adsorption isotherm. Thus, the correlation of equilibrium data by either theoretical or empirical model is essential to practical operation. Langmuir and Freundlich's equations were used to analysis the experimental data of the MMWCNTs adsorbents for phosphate in our work.

3.5.1. Langmuir isotherm

The Langmuir isotherm model assumes monolayer coverage on a homogeneous surface without interaction between adsorbed molecules and uniform energies of adsorption onto the surface [27]. The linear form of Langmuir isotherm equation is given by:

$$\frac{C_e}{q_e} = \frac{C_e}{q_m} + \frac{1}{K_l q_m} \quad (5)$$

where C_e is the equilibrium phosphate concentration (mg·l^{-1}), q_e is the amount of phosphate adsorbed at equilibrium (mg/g), K_L is constant and q_m is the maximum amount of phosphate adsorbed (mg.g^{-1}). The Langmuir adsorption isotherm results are given in Table 5. As can be observed, the equilibrium data are well displayed by Langmuir adsorption isotherm, with maximum monolayer adsorption capacity of 263 mg·g^{-1} for the MMWCNT. The essential characteristics of Langmuir isotherm can be expressed in terms of a dimensionless equilibrium parameter (R_L). This parameter is defined as:

$$R_L = \frac{1}{1 + K_L C_0} \quad (6)$$

where K_L is the Langmuir constant and C_0 is the highest initial adsorbate concentration (mg·l^{-1}). The value of R_L indicates type of the isotherm to be either unfavorable ($R_L > 1$), linear ($R_L = 1$), favorable ($0 < R_L < 1$) or irreversible ($R_L = 0$). As can be observed in Table 5, the dimensionless constant values, R_L, lie within the favorable limit for adsorption of phosphate onto the MMWCNT [27].

3.5.2. Freundlich isotherm

The Freundlich isotherm model is an experimental equation employed to describe the multilayer adsorption with a heterogeneous energetic distribution of active sites, accompanied by interactions between adsorbed molecules [27]. The well-known logarithmic form of Freundlich isotherm equation is given by Eq. (7):

$$\log q_e = \log K_F + \left(\frac{1}{n}\right) \log C_e \quad (7)$$

where C_e is the equilibrium phosphate concentration (mg·l^{-1}), q_e is the amount of phosphate adsorbed equilibrium (mg·g^{-1}), K_F and n are the Freundlich constants. The parameters of Eqs. (5)–(7) were computed and are presented in Table 5. As shown, Table 5 includes four initial concentration range. Higher initial concentration range (125–166.67 mg/l), Moderate initial concentration range (85–125 mg/l), lower initial concentration range (40–85 mg/l) and whole initial concentration range (40–166.67 mg/l). These indicate that Langmuir adsorption isotherm is found more suitable only to moderate initial concentrations (85–125 ppm and $R^2 = 0.9938$). Therefore, the Langmuir isotherm correlates better than the Freundlich isotherm with the experimental data, indicating the adsorbed phosphate does not interact with each other and the adsorption of phosphate by MWCNTs/Fe_3O_4 nanocomposites is a monolayer adsorption. The linear plots for Langmuir and Freundlich isotherms in four ranges of initial concentration are shown in Figs. 9–11.

The effect of initial concentration on adsorption of phosphate was investigated in the range of (85–125 mg/l) or

Table 5
Langmuir and Freundlich isotherm model parameters and correlation coefficients for adsorption of phosphate onto MMWCNT

Adsorbent (MMWCNT)	Langmuir isotherm model				Freundlich isotherm model		
	q_m(mg/g)	K_L(l/mg)	R_L	R^2	Log(K_F)	1/n	R^2
Whole con.	285	0.199	0.029	0.9778	2.5756	0.0783	0.6692
Low con.	238	0.333	0.035	0.9927	2.6072	0.1109	0.9076
Mod con.	278	0.111	0.067	0.9938	2.2243	0.0887	0.6540
High con.	625	0.007	0.465	0.9886	1.3952	0.5055	0.9906

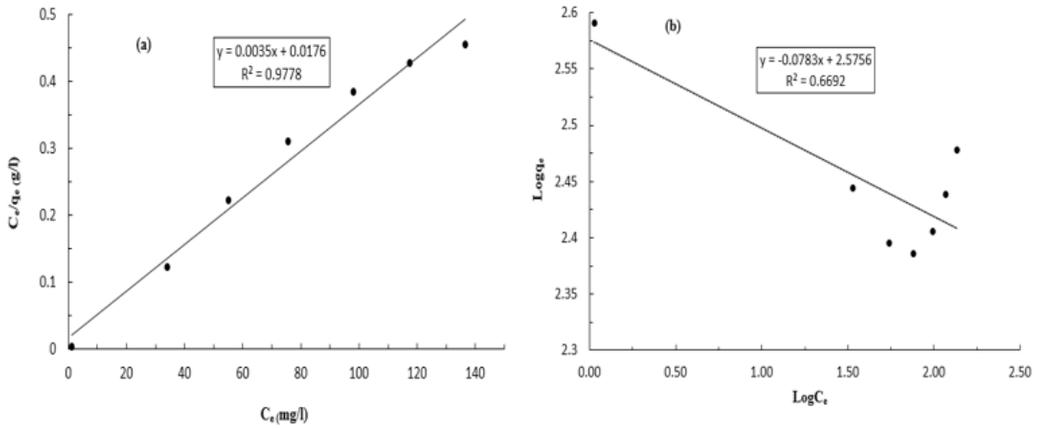

Fig. 9. Adsorption isotherms for the whole initial concentration range of phosphate onto MMWCNTs at different initial concentration: Langmuir (a) and Freundlich (b). (Volume of phosphate solution: 50 mL, initial concentration of phosphate: 40–166.67 mg/L, adsorbent: 5 mg, pH: 4).

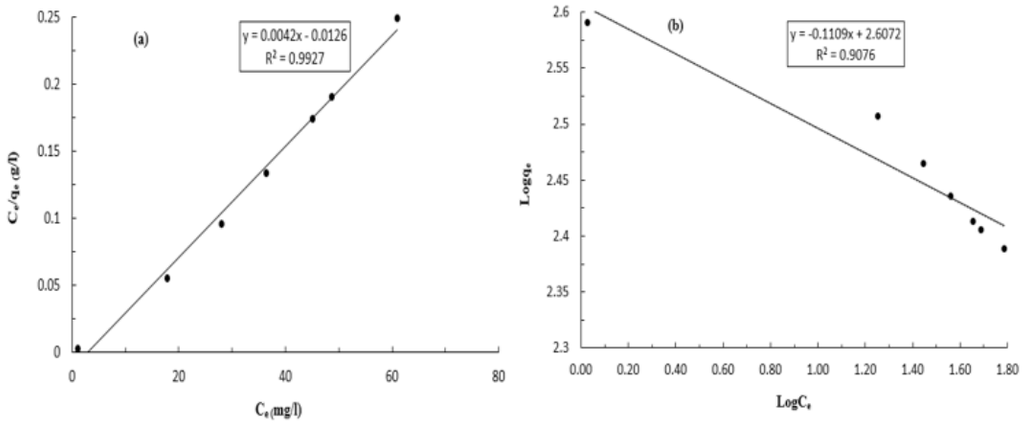

Fig. 10. Adsorption isotherms for low initial concentration range of phosphate onto MMWCNTs at different initial concentration: Langmuir (a) and Freundlich (b). (volume of phosphate solution: 50 mL, initial concentration of phosphate: 40 –85 mg/L, adsorbent: 5 mg, pH: 4).

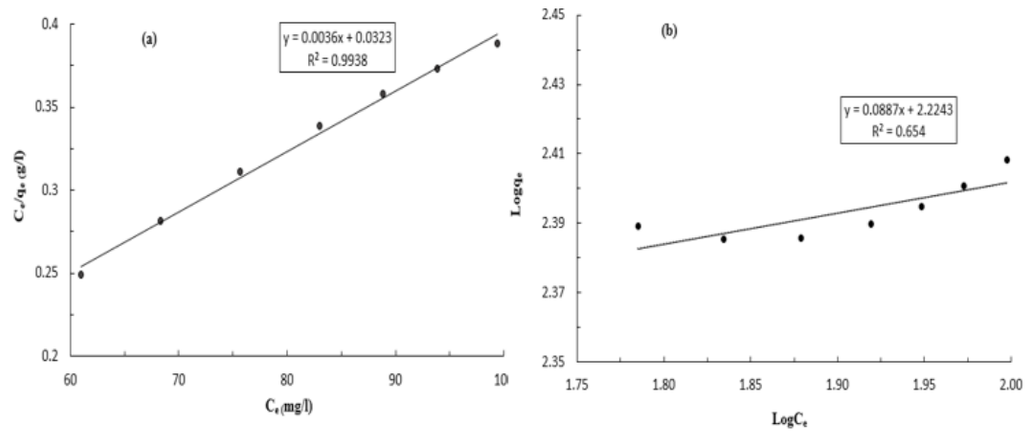

Fig. 11. Adsorption isotherms for moderate initial concentration range of phosphate onto MMWCNTs at different initial concentration: Langmuir (a) and Freundlich (b). (volume of phosphate solution: 50 mL, initial concentration of phosphate: 85–125 mg/L, adsorbent: 5 mg, pH: 4).

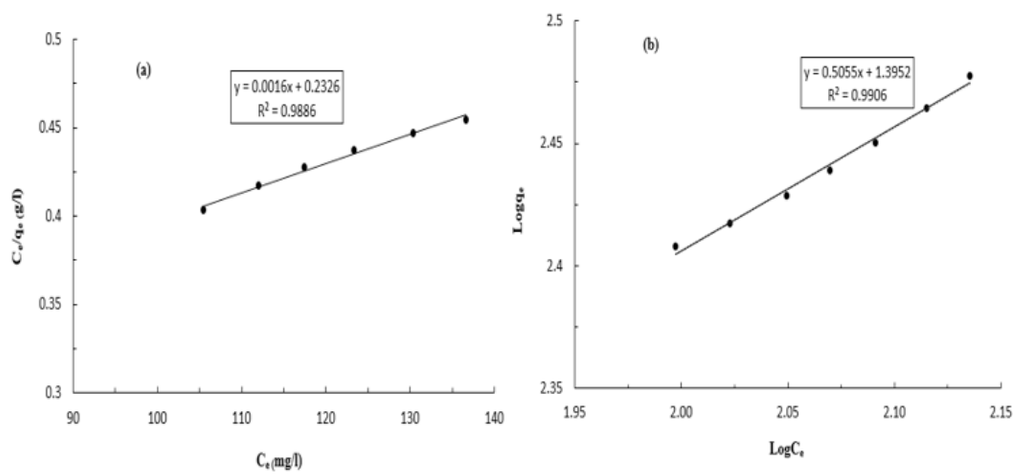

Fig. 12. Adsorption isotherms for the high initial concentration range of phosphate onto MMWCNTs at different initial concentration: Langmuir (a) and Freundlich (b). (Volume of phosphate solution: 50 mL, initial concentration of phosphate: 125 –166.67 mg/L, adsorbent: 5 mg, pH: 4).

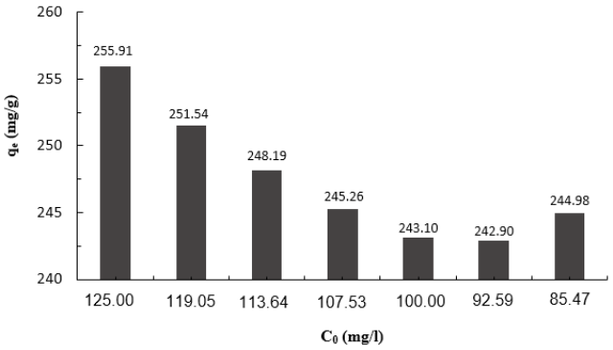

Fig. 13. Equilibrium adsorption uptake of phosphate for MMWCNT at different initial concentration and pH 4.

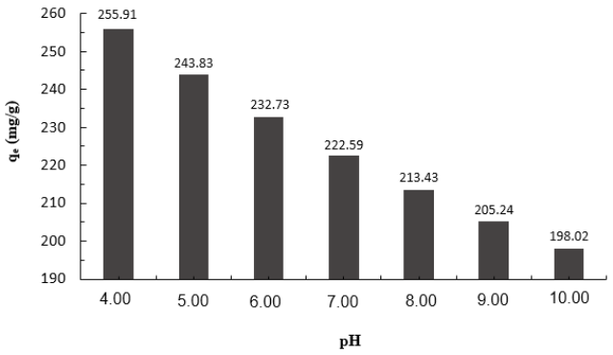

Fig. 14. Equilibrium adsorption uptake of phosphate for MMWCNT at different pH and initial concentration 125 mg/l.

D/C (0.8–1.19) at pH 4. Results were presented in Fig. 13. It indicated that the adsorption capacity of MMWCNTs increases up to approximately 256 mg·g^{-1}. Fig. 14 observed that phosphate uptake reduces with an increase in solution pH from 4 to 10. This can be due to the negative charge of the surface of MMWCNTs in a high pH range. The negative charge of the surface of the magnetic carbon nanotubes was also confirmed from the data on the zeta potential [28]. With the increasing of pH, the adsorption capacity decreased. In particular, the strong electrostatic attraction was revealed on the surface of the positively charged adsorbent in low pH due to the negatively charged phosphate and the relaxation of the functional group [29]. At higher pH, the negatively charged parts also increased, but the electrostatic repulsion from the negatively charged parts of the adsorbent does not favor absorption of phosphate [30]. Fig. 14 indicated that lower adsorption capacity was at the higher pH. The MMWCNTs were positively charged at pH 4.00. Thus, the increases adsorption of phosphate at lower pH values (pH = 4.00) could be due to the reduced electrostatic repulsion between the phosphate anion and the positively charged on MMWCNTs.

4. Conclusion

In this study, a successful synthetic method to prepare stable MMWCNTs without using highly toxic chemicals is reported. The prepared MMWCNTs is well dispersed in the water and can be easily separated magnetically from the solution after adsorption. In this study, The MMWCNT was successfully adsorbed for phosphate removal. The modeling and the optimization of the removal of phosphate were performed by using response surface methodology–central composite design (RSM–CCD). Two parameters, namely pH and D/C were the control factors in this study. One quadratic model removal phosphate was developed. Analyze of variance results confirmed that there was a significant agreement between the models and the experimental data. The results show that pH and D/C were the factors with statistically high significant effect. The optimum point was found at pH = 4 and (D/C) = 2.50 with the predicted removal of 97.35%. Langmuir isotherm model of phosphate adsorption on MMWCNTs with high correlation coefficient is a better fit than Freundlich isotherm model.

References

[1] S. Water, W.H. Organization, Guidelines for drinking-water quality [electronic resource]: incorporating first addendum. Vol. 1, Recommendations. 2006.
[2] V. Alimohammadi, M. Sedighi, E. Jabbari, Response surface modeling and optimization of nitrate removal from aqueous solutions using magnetic multi-walled carbon nanotubes. J. Environ. Chem. Eng., 4(4) (2016) 4525–4535.
[3] N. Tran, P. Drogui, J.-F. Blais, G. Mercier, Phosphorus removal from spiked municipal wastewater using either electrochemical coagulation or chemical coagulation as tertiary treatment, Separ. Purif. Technol., 95 (2012) 16–25.
[4] S. Rasoul-Amini, N. Montazeri-Najafabady, S. Shaker, A. Safari, A. Kazemi, P. Mousavi, M.A. Mobasher, Y. Ghasemi, Removal of nitrogen and phosphorus from wastewater using microalgae free cells in bath culture system, Biocatal. Agric. Biotechnol., 3(2) (2014) 126–131.
[5] J. Xiong, Q. Mahmood, Adsorptive removal of phosphate from aqueous media by peat, Desalination, 259(1) (2010) 59–64.
[6] Z. Zhang, H. Li, J. Zhu, L. Weiping, X. Xin, Improvement strategy on enhanced biological phosphorus removal for municipal wastewater treatment plants: Full-scale operating parameters, sludge activities, and microbial features, Bioresour. Technol. 102(7) (2011) 4646–4653.
[7] R. Li, Z. Lin, T. Tao, L. Bo, Phosphorus removal performance of acid mine drainage from wastewater, J. Hazard. Mater., 190(1) (2011) 669–676.
[8] Y. Yao, B. Gao, M. Inyang, A.R. Zimmerman, X. Cao, P. Pullammanappallil, L. Yang, Removal of phosphate from aqueous solution by biochar derived from anaerobically digested sugar beet tailings, J. Hazard. Mater., 190(1) (2011) 501–507.
[9] A. Arab Markadeh, A. Rezaee, S.O. Rastegar, H. Hossini, S. Ahmadi, E. Hoseinzadeh, Optimization of Remazol Brilliant Blue adsorption process from aqueous solutions using multi-walled carbon nanotube, Desal. Water Treat., 57(28) (2016) 13357–13365.
[10] T. Madrakian, A. Afkhami, M. Ahmadi, H. Bagheri, Removal of some cationic dyes from aqueous solutions using magnetic-modified multi-walled carbon nanotubes, J. Hazard. Mater., 196 (2011) 109–114.
[11] N.Y. Acelas, B.D. Martin, D. López, B. Jefferson, Selective removal of phosphate from wastewater using hydrated metal oxides dispersed within anionic exchange media, Chemosphere, 119 (2015) 1353–1360.
[12] Q. Zhou, X. Wang, J. Liu, L. Zhang, Phosphorus removal from wastewater using nano-particulates of hydrated ferric oxide doped activated carbon fiber prepared by Sol–Gel method, Chem. Eng. J., 200 (2012) 619–626.

[13] J.H. Park, D.I. Jung, Removal of total phosphorus (TP) from municipal wastewater using loess, Desalination, 269(1) (2011) 104–110.
[14] K. Yang, Z. Li, H. Zhang, J. Qian, G. Chen, Municipal wastewater phosphorus removal by coagulation, Environ. Technol., 31(6) (2010) 601–609.
[15] J.-G Yu, X.-H. Zhao, H. Yang, X.-H. Chen, Q. Yang, L.-Y. Yu, J.-H. Jiang, X.-Q. Chen, Aqueous adsorption and removal of organic contaminants by carbon nanotubes, Sci. Total Environ., 482 (2014) 241–251.
[16] S. Qu, F. Huang, S. Yu, G. Chen, J. Kong, Magnetic removal of dyes from aqueous solution using multi-walled carbon nanotubes filled with Fe_2O_3 particles, J. Hazard. Mater., 160(2) (2008) 643–647.
[17] F. Yu, J. Ma, J. Wang, M. Zhang, J. Zheng, Magnetic iron oxide nanoparticles functionalized multi-walled carbon nanotubes for toluene, ethylbenzene and xylene removal from aqueous solution, Chemosphere, 146 (2016) 162–172.
[18] E. Deliyanni, E. Peleka, K. Matis, Removal of zinc ion from water by sorption onto iron-based nanoadsorbent. J. Hazard. Mater., 141(1) (2007) 176–184.
[19] C. Liu, R. Bai, Q.S. Ly, Selective removal of copper and lead ions by diethylenetriamine-functionalized adsorbent: Behaviors and mechanisms, Water Res., 42(6) (2008) 1511–1522.
[20] I. Mobasherpour, E. Salahi, M. Ebrahimi, Removal of divalent nickel cations from aqueous solution by multi-walled carbon nano tubes: equilibrium and kinetic processes, Res. Chem. Intermed., 38(9) (2012) 2205–2222.
[21] J. Perić, M. Trgo, N.V. Medvidović, Removal of zinc, copper and lead by natural zeolite—a comparison of adsorption isotherms, Water Res., 38(7) (2004) 1893–1899.
[22] S. Yang, J. Li, D. Shao, J. Hu, X. Wang, Adsorption of Ni (II) on oxidized multi-walled carbon nanotubes: effect of contact time, pH, foreign ions and PAA, J. Hazard. Mater., 166(1) (2009) 109–116.
[23] V. Alimohammadi, M. Sedighi, E. Jabbari, Experimental study on efficient removal of total iron from wastewater using magnetic-modified multi-walled carbon nanotubes, Ecol. Eng., 102 (2017) 90–97.
[24] M. Zhang, Y. Wu, Y. Fan, W. Zhu, H. Zhao, A. Arkin, Evaluation of the mesoporous silica material MCM-41 for competitive adsorption of Basic Violet 5BN and Basic Green from industrial dye wastewater, Desal. Water Treat., 57(37) (2016) 17494–17511.
[25] L. Kong, X. Lu, W. Zhang, Facile synthesis of multifunctional multiwalled carbon nanotubes/Fe_3O_4 nanoparticles/polyaniline composite nanotubes, J. Solid State Chem., 181(3) (2008) 628–636.
[26] Z.-H. Wang, B.-Y. Yue, J. Teng, F.-P. Jiao, X.-Y. Jiang, J.-G. Yu, M. Zhong, X.-Q. Chen, Tartaric acid modified graphene oxide as a novel adsorbent for high-efficiently removal of Cu (II) and Pb (II) from aqueous solutions, J. Taiwan Inst. Chem. Eng., 66 (2016) 181–190.
[27] M.A. Tofighy, T. Mohammadi, Nitrate removal from water using functionalized carbon nanotube sheets, Chem. Eng. Res. Design, 90(11) (2012) 1815–1822.
[28] M. Legodi, D. De Waal, The preparation of magnetite, goethite, hematite and maghemite of pigment quality from mill scale iron waste, Dyes Pigments, 74(1) (2007) 161–168.
[29] P. Velmurugan, J. Shim, B.-T. Oh, Removal of anionic dye using amine-functionalized mesoporous hollow shells prepared from corn cob silica. Res. Chem. Intermed. (2016) 1–14.
[30] S. Debnath, A. Maity, K. Pillay, Impact of process parameters on removal of Congo red by graphene oxide from aqueous solution, J. Environ. Chem. Eng., 2(1) (2014) 260–272.